

Structural Phase Transitions in SrRh₂As₂

V. Zinth¹, V. Petricek², M. Dusek², and D. Johrendt*¹

¹ *Department of Chemistry, Ludwig-Maximilians-Universität, 81377 München, Germany*

² *Institute of Physics, Cukrovarnicka 10, 16253 Praha, Czech Republic*

SrRh₂As₂ exhibits structural phase transitions reminiscent to those of BaFe₂As₂, but crystallizes with three polymorphs derived from the tetragonal ThCr₂Si₂-type structure. The structure of α -SrRh₂As₂ is monoclinic with $a = 421.2(1)$ pm, $b = 1105.6(2)$ pm, $c = 843.0(1)$ pm and $\beta = 95^\circ$ and was refined as a partially pseudo merohedric twin in the space group $P2_1/c$ with $R1 = 0.0928$. β -SrRh₂As₂ crystallizes with a modulated structure in the (3+1) dimensional superspace group $Fmmm(10\gamma)\sigma 00$ with the unit cell parameters $a = 1114.4(3)$ pm, $b = 574.4(2)$ pm and $c = 611.5(2)$ pm and an incommensurable modulation vector $\mathbf{q} = (1, 0, 0.3311(4))$. High temperature single crystal diffraction experiments confirm the tetragonal ThCr₂Si₂-type structure for γ -SrRh₂As₂ above 350°C. Electronic band structure calculations indicate that the structural distortion in α -SrRh₂As₂ is caused by strong Rh-Rh bonding interactions and has no magnetic origin as suggested for isotypic BaFe₂As₂.

PACS 61.66.Fn 61.50.Ks 61.44.Fw 74.62.Bf

I. Introduction

The coupling of electronic and lattice degrees of freedom creates some of the most intriguing phenomena in solid state materials. Two well known manifestations of electron-lattice coupling are charge-/spin-density-waves (CDW, SDW)¹ and conventional superconductivity.² In superconductors, the coupling is usually weak, but it determines the critical temperature T_c . Stronger coupling increases T_c to a certain limit, while too strong interactions can drive the system to a CDW state, where a structural distortion reduces the electronic energy.

Structural phase transitions associated to CDW instabilities have been observed in many metallic materials with quasi low-dimensional crystal structures, among them transition-metal chalcogenides^{3,4} and oxides.⁵ CDW ordering has often been considered as a manifestation of the Peierls-instability, thus relying on nesting, which means that a piece of the Fermi surface can be translated by a vector \mathbf{q} and superimposed on another piece of the surface. Meanwhile, reasonable doubts arise whether nesting is the only driving force of the CDW, and in fact, \mathbf{q} -vectors extracted from Fermi surface nesting are in some cases inconsistent with experimental wave vectors,⁶ even in the archetypical CDW compound TaSe₂.⁷

Layered crystal structures also constitute the basis of the high-temperature superconductors, both the copper oxides⁸ and the iron arsenides.^{9,10} The latter are build up by layers of edge-sharing

FeAs₄-tetrahedra, separated either by oxide layers as in LaOFeAs with ZrCuSiAs-type structure¹¹ or by alkaline earth metals as in BaFe₂As₂ with ThCr₂Si₂-type structure.¹² These non-superconducting parent compounds exhibit SDW-type phase transitions, accompanied by a reduction of the space group symmetry from tetragonal to orthorhombic.^{13,14} In these materials, the SDW wave vectors perfectly coincide with the Fermi surface nesting, which is also believed to play a certain role in the pairing mechanism.¹⁵

The orthorhombic low-temperature structure of BaFe₂As₂ was first classified¹⁶ as isotypic to the β -SrRh₂As₂-type in the space group *Fmmm*.¹⁷ Indeed also rhodium compound transforms to the tetragonal ThCr₂Si₂-type (γ -SrRh₂As₂, space group *I4/mmm*), but at much higher temperature (555 K) in comparison with BaFe₂As₂ (140 K)¹⁴ and SrFe₂As₂ (210 K).¹⁸ Furthermore, the orthorhombic lattice distortion, measured as $\delta = |a-b|/(a+b)$, is about one order of magnitude larger in SrRh₂As₂ ($\delta \approx 10^{-2}$) than in BaFe₂As₂ ($\delta \approx 10^{-3}$). Despite the striking symmetry congruence of the *I4/mmm* \leftrightarrow *Fmmm* structural transitions in SrRh₂As₂ and BaFe₂As₂, both are not expected to have the same origin. Since SrRh₂As₂ carries no magnetic moment, the driving force is not magneto-elastic coupling by antiferromagnetic SDW ordering as in BaFe₂As₂. Thus, the $\beta \rightarrow \gamma$ transition of SrRh₂As₂ may be assigned to a possible CDW instability of the RhAs_{4/4} layers. However, recently published band structure calculations¹⁹ revealed no hint to an instability, however, the electronic susceptibility has not yet been analyzed in detail. Furthermore, β -SrRh₂As₂ transforms to a third (α -) modification, which is stable below 555 K. The structure of α -SrRh₂As₂ was assumed to be closely related to the orthorhombic BaNi₂Si₂-type (space group *Cmcm*), but could not be successfully refined.

In order to shed light on several open issues regarding the crystal structures and phase transitions of polymorphic SrRh₂As₂ and its relationships to those occurring in the isostructural iron arsenides, we have synthesized SrRh₂As₂ and conducted detailed single crystal X-ray experiments.

II. Experimental Details

Powder samples of α -SrRh₂As₂ were synthesized by heating stoichiometric mixtures of the elements in alumina crucibles that were sealed in silica tubes under an atmosphere of purified argon. The mixtures were heated to 620 °C, kept at this temperature for 10 h and cooled down to room temperature. The reaction products were homogenized and annealed at 1000 °C for 30 hours several times. X-ray powder patterns have been measured on a STOE Stadi-P diffractometer (Cu-K _{α 1} radiation). The TOPAS²⁰ package was used for Rietveld refinements. The powder diffraction pattern of α -SrRh₂As₂ together with the Rietveld refinement are shown in Fig. 1.

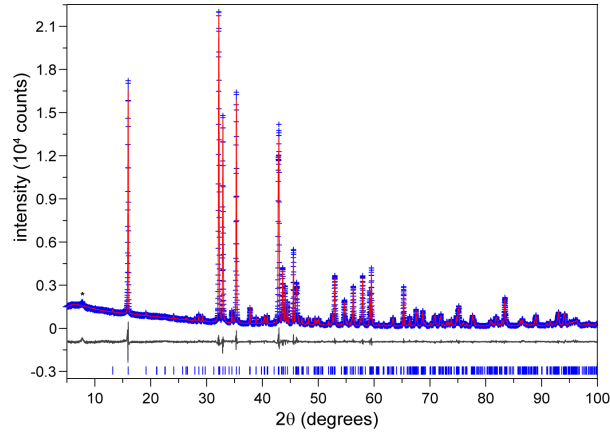


FIG. 1. X-ray powder pattern and Rietveld refinement of α - SrRh_2As_2

Single crystals of α - SrRh_2As_2 were grown in a Pb/Bi-flux (55 wt % Bi, ten times surplus of flux) by heating to 1100 °C, holding the temperature for 30 h, cooling to 160 °C with 2 °C/h and then quenching the sample. Single crystals of β - SrRh_2As_2 were obtained in a similar way using 45 wt % Bi and a cooling rate of 30 °C/h. The flux was dissolved in HAc/H₂O₂, and revealed platelike crystals with a tendency to cleave. The crystals were checked by Laue photographs using white molybdenum radiation. Single crystal intensity data of α - and γ - SrRh_2As_2 was recorded on a STOE IPDS imaging plate detector (Ag-K α , graphite monochromator, ϕ -scan) equipped with a Heatstream (Stoe & Cie GmbH, Darmstadt, Germany) device for high temperature measurements. Single crystal intensity data of β - SrRh_2As_2 was collected on a Gemini four-circle diffractometer equipped with an Atlas CCD detector. For structure solution and refinement the SHELX suite of programs²¹⁻²² (α - SrRh_2As_2 and γ - SrRh_2As_2) and the program Jana2006²³ (β - SrRh_2As_2) were used. The electronic structure and Crystal Orbital Hamilton Function (COHP) of α - SrRh_2As_2 and γ - SrRh_2As_2 were calculated from self-consistent TB-LMTO-ASA²⁴ potentials and wave functions²⁵ using density-functional (DFT) methods

III. Results

A Crystal structures

1. α - SrRh_2As_2

Diffraction patterns of the room temperature phase pretended orthorhombic mmm symmetry as reported in Ref.¹⁷, but all attempts at finding a satisfactory structure model failed. A careful inspection of the pattern revealed multiple twinning, but only two main domains contribute considerably as shown in Figure 2a. Their unit cell dimensions are $a = 421.2(1)$ pm, b

= 1105.6(2) pm, $c = 843.0(1)$ pm and $\beta = 95^\circ$, respectively. The latter is supported by observations in single crystals of α -SrRh₂As₂ with about 10 % of Sr substituted by Ba, where an easier kind of twinning occurs and the unit cell dimensions can easily be identified. The domains shown in figure 2a transform onto each other by a twofold rotation around [1 0 2] that feigns the two times larger pseudo unit cell $a \approx 842$ pm, $b \approx 1106$ pm, $c \approx 842$ pm and $\beta = 95^\circ$. or a four times larger pseudo-orthorhombic unit cell with $A = -2a - c = 1138$ pm, $B = -b = 1105.6$ pm, $C = -2a + c = 1243.2$ pm, $\alpha = 90^\circ$, $\beta = 90.04^\circ$, $\gamma = 90^\circ$. Integration of the intensity data was performed using this doubled monoclinic pseudo unit cell. An absorption correction was performed using the shape of the crystal as obtained by the diffractometer's video system. Then the reflections were transformed according to the two domains, stored into a .hklf5 file and merged with the program mergehklf5²⁶. The structure was solved and refined in the space group $P2_1/c$ with $R1 = 0.0928$ (Table 1).

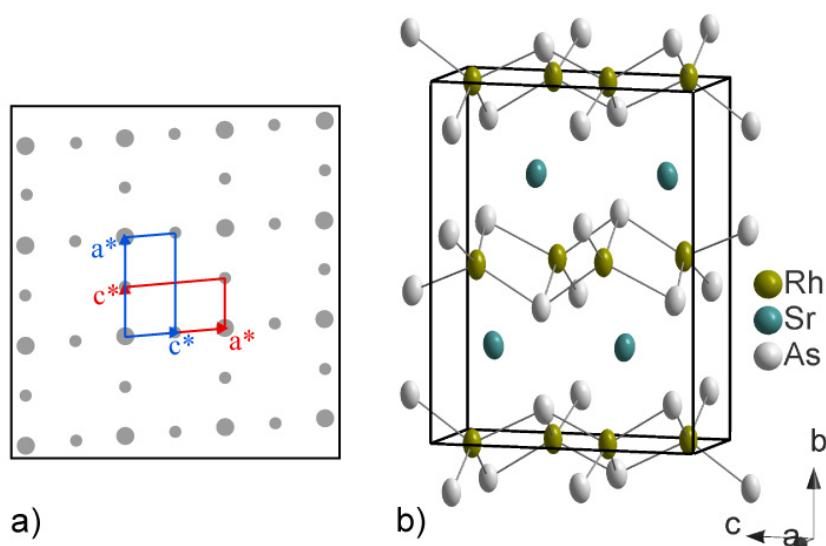


FIG. 2. a) Schematical picture of the reciprocal space of α -SrRh₂As₂ with the unit cells of the two twin domains, b) unit cell of α -SrRh₂As₂, the anisotropic atomic displacement parameters (95 % probability) are shown

Selected interatomic distances and bond angles of α -SrRh₂As₂ are compiled in Table 2. The shortest As-As distances between the RhAs₄-tetrahedron layers is 313.0 pm, thus no significant interlayer bonding is expected. The Rh-As distances range from 238.8 to 251.1 pm and the As-Rh-As angles in the RhAs₄-tetrahedra from 79.24° to 123.89°. The strong distortions of the RhAs₄-tetrahedron layers are visible in Fig. 2b, which shows the unit cell of α -SrRh₂As₂. The distortion is best be grasped by looking at the positions of the Rh atoms within the RhAs-layers (Fig. 3). In contrast to the regular square network of Rh in the tetragonal high temperature phase with a constant distance of 290 pm between the Rh atoms, Rh-Rh distances in α -SrRh₂As₂ vary from 284.7 pm to 378.5 pm, and chains of four Rh atoms with short distances alternating with one longer distance between the chains.

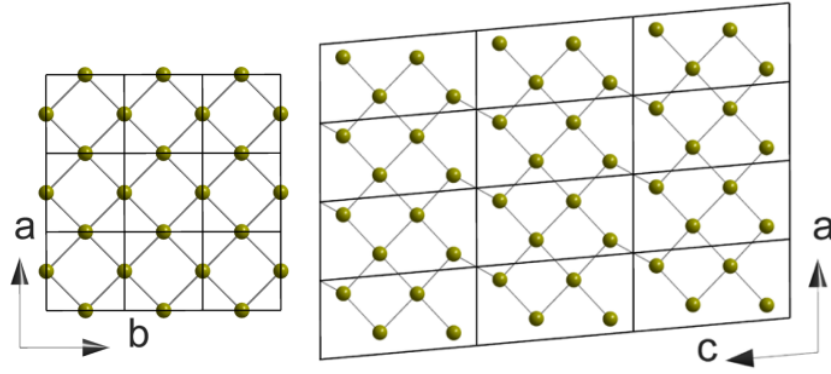


FIG. 3. Comparison of the rhodium networks in γ - (left) and α - SrRh_2As_2 (right)

Table 1 crystallographic data of α - SrRh_2As_2

Empirical formula	SrRh_2As_2
Crystal system, space group	Monoclinic, $P 2_1/c$, No. 14
a, b, c (pm), β ($^\circ$)	421.2(1), 1105.6(2), 843.0(1), 95.06(2)
Cell volume (nm^3)	0.3920(1)
Molar mass (g/mol)	443.3
Calculated density (g/cm^3), Z	7.53, 4
Radiation type, λ (\AA)	Ag- K_α , 0.56087
2θ range	4.6 - 60.9
Transmission (min, max)	0.1960, 0.5600
Absorption coefficient (mm^{-1})	20.46
Total number of reflections	12430
Independent reflections, R_{meas}	3652, 0.2188
Reflections with $I > 2\sigma(I)$, R_σ	1582, 0.1545
Refined parameters, Goodness-of-Fit on F^2	47, 0.86
$R1, wR2$ ($I > 2\sigma(I)$)	0.0928, 0.2312
$R1, wR2$ (all data)	0.1891, 0.3107
Largest residual peak, hole $e/\text{\AA}^3$	5.654, -6.042
Twin fraction	51.7(3) %
Atomic parameters	
	x y z U_{eq}
Sr 4e	0.2478(4) 0.7539(1) 0.1341(2) 0.0184(3)
Rh1 4e	0.2245(3) 0.5067(2) 0.3807(2) 0.0166(3)
Rh2 4e	0.3116(4) 0.0093(2) 0.3522(2) 0.0179(3)
As1 4e	0.1868(4) 0.4072(2) 0.1126(2) 0.0185(3)
As2 4e	0.2749(4) 0.1229(2) 0.1108(2) 0.0171(3)

Table 2 interatomic distances (pm) and angles in α -SrRh₂As₂

Rh1 -	Distance	Rh2 -	Distance	Sr3 -	Distance
As4	240.8(2)	As4	238.8(2)	As4	317.0(2)
As4	246.4(2)	As5	239.1(2)	As4	319.4(2)
As4	247.0(2)	As5	242.4(2)	As5	319.5(2)
As5	251.1(2)	As5	248.3(2)	Rh2	327.8(2)
Rh2	286.4(3)	Rh2	284.7(3)	As4	330.1(2)
Rh1	288.4(2)	Rh1	286.4(3)	Rh2	337.1(2)
Rh2	289.0(2)	Rh1	288.8(2)	As5	338.8(2)
Rh1	294.3(3)			Rh1	340.1(2)
				Rh1	342.8(2)
As5 -				Rh1	344.4(2)
As5	313.0(1)				
As4	317.0(1)				
Angle					
As4-Rh1-As4		105.68(8)	As4-Rh2-As5		110.23(7)
As4-Rh1-As4		107.53(7)	As4-Rh2-As5		110.89(8)
As4-Rh1-As5		117.5(1)	As4-Rh2-As5		123.89(9)
As4-Rh1-As4		117.2(1)	As5-Rh2-As5		122.0(1)
As4-Rh1-As5		104.02(7)	As5-Rh2-As5		108.54(8)
As4-Rh1-As5		105.46(8)	As5-Rh2-As5		79.24(8)

2. β -SrRh₂As₂

First measurements of β -SrRh₂As₂ single crystals revealed orthorhombic all face centered symmetry with unit cell parameters $a = 1114.4(3)$ pm, $b = 574.4(2)$ pm and $c = 611.5(2)$ pm in agreement with Ref.¹⁷. An initial refinement using the space group $Fmmm$ converged to $R1 = 0.055$, but the anisotropic displacement parameters were not acceptable and clearly hint at a lower symmetry. The inspection of the diffraction pattern revealed additional satellite spots surrounding each Bragg position of the orthorhombic cell as shown in Fig. 4. These strong satellite reflections were indexed using the nearly commensurable modulation vector $\mathbf{q} = (1, 0, \approx 1/3)$. Additional, very weak spots were detected at $\mathbf{q} = (0.5, 0, \approx 1/6)$ and further, barely detectable reflections exist for some $(h+1/2, k, l+1/2)$ (possibly 3rd order satellites) and $(h, k+1/2, l+1/2)$. Using the $(0.5, 0, \approx 1/6)$ reflections as first order satellites, we have the rather unusual case that the second order satellites are much stronger than the first order ones. This clearly indicates that the second order components of the modulation functions are predominant. As a first approach, we have neglected the weak first order spots and tried to find a solution using $\mathbf{q} = (1, 0, 0.3311(4))$ as the modulation vector, which is compatible with the $(3+1)$ -dimensional superspace group $Fmmm(10\gamma)\sigma 00$.

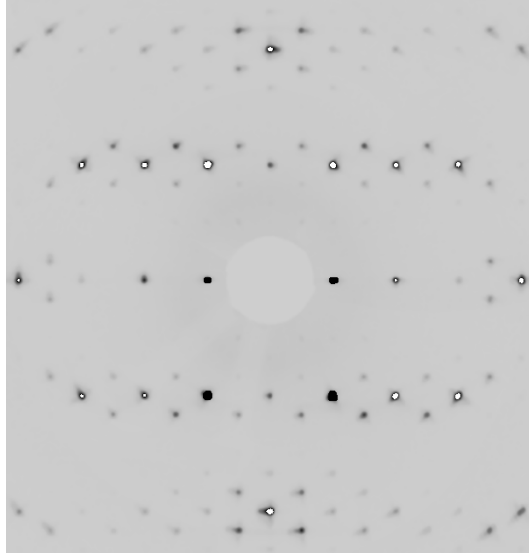


FIG. 4. h0l-layer of β -SrRh₂As₂ with strong satellite spots at $\mathbf{q} = (1, 0, 0.3311(4))$.

A comparison of the lattice parameters shows similarities between the above mentioned pseudo orthorhombic lattice A, B, C of α -SrRh₂As₂ and the cell parameters of β -SrRh₂As₂ ($a \approx A, b \approx B/2, c \approx C/2$). Thus it seems possible that the α -phase is still partially present in the crystal of the β -phase. This would cause additional reflections with $(h, k+1/2, l+1/2)$ and violations of the F -centering, both of which we observe. A multiphase refinement of the crystal gives a significantly better fit for the collected data and yields a volume fraction of 68 % β -phase and 16 % for each of the α -phase twin components. The refinement data are summarized in Tables 3, 4 and 5. The \mathbf{q} -vector is close to commensurable, but the best refinement results were obtained with the incommensurate model. The overlap option for closest reflections implemented in Jana2006 was used. Both first and second order satellite reflections are reasonably well refined (see Table. 3).

The strongest modulation concerns the position of the Rh-atom in c -direction (Fig. 5a). A crenel function was used to describe the modulation, combined with a positional modulation function expressed by Legendre polynomial. No modulation of the Rh atoms in a - and b - directions were observed. The strong modulation of the Rh atom influences the adjoining As atom, which shows a positional modulation in c - direction that can be described very well by a combination of one sinus and one cosinus term (Fig 5b). For the As atom also a second positional modulation with smaller amplitude is observed in a - direction (Fig 6a). The Sr atoms show pretty much the same modulation in a -direction (Fig. 6b). The modulation function of the ADP parameters was also refined, with the biggest changes found for the ADP parameters of the As atom (see Table 4).

Table 3 crystallographic data of β -SrRh₂As₂

Empirical formula	SrRh ₂ As ₂
Crystal system, space group	orthorhombic, Fmmm(10 γ) σ 00
a, b, c (pm)	1114.4(3), 574.4(2), 611.5(2)
Cell volume (nm ³)	0.3914 (2)
Molar mass (g/mol)	443.3
Calculated density (g/cm ³), Z	7.52, 4
Radiation type, λ (Å)	Mo-K α , 0.7107
2θ range	5.7272 - 58.6562
Transmission (min, max)	0.23117, 1.000
Absorption coefficient (mm ⁻¹)	38.425
Total number of reflections	23001
Independent reflections, R_{int}	1271, 0.0470
Reflections with $I > 3\sigma(I), R_{\sigma}$	833, 0.0105
Main reflections: $I > 3\sigma(I)$ / all	327/ 479
1. order satellites: $I > 3\sigma(I)$ / all	225/ 258
2. order satellites: $I > 3\sigma(I)$ / all	281/ 534
Refined parameters, GooF	47, 5.90
$R(obs)(I > 3\sigma(I))/R(obs)(all)$	0.0563/ 0.0918
Main reflections	0.0424/ 0.0567
1. order satellites	0.0569/ 0.0658
2. order satellites	0.0911/ 0.1952
$wR(I > 3\sigma(I))/wR(all)$	0.1089/ 0.1260
Main reflections	0.0982/ 0.0991
1. order satellites	0.1045/ 0.1054
2. order satellites	0.1364/ 0.1942
Residual peak, hole $e^{-}/\text{Å}^3$	6.67/-5.66

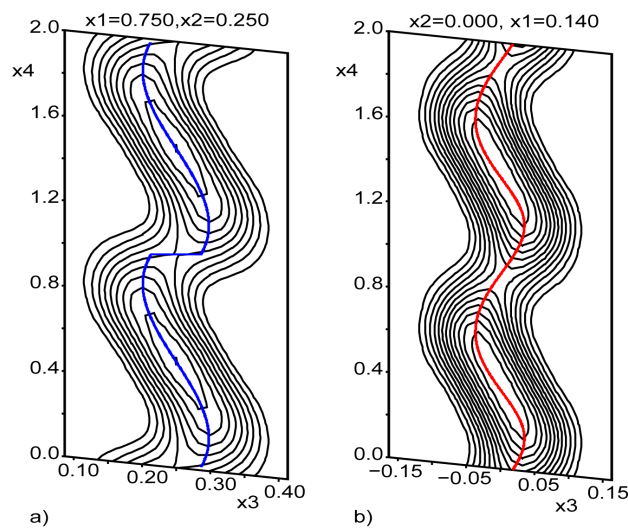


FIG. 5. Fourier map with a) positional modulation of Rh in c -direction, b) of As in c -direction

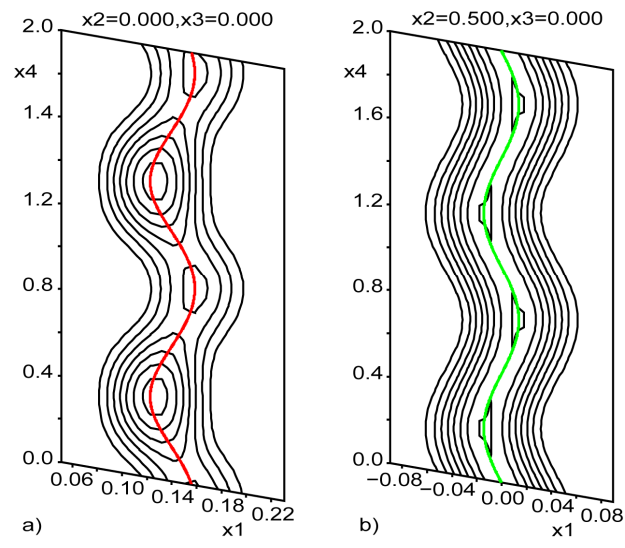


FIG. 6. Fourier map with a) Positional modulation of As in a -direction, b) of Sr in a -direction.

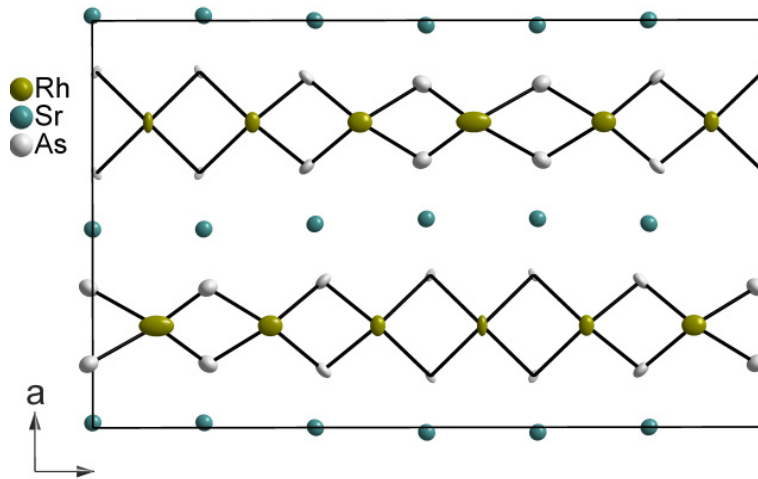


FIG. 7. Modulated structure of β - SrRh_2As_2 , projection along b .

Table 4 parameters of the modulation functions of β -SrRh₂As₂

Atom	x, y, z	U ₁₁	U ₂₂	U ₃₃
Rh, 8d	0.75, 0.25, 0.25	0.0252(7)	0.0083(5)	0.0282(7)
Sr 4d	0, 0.5, 0	0.0163(11)	0.0103(12)	0.0174(10)
As 8d	0.1410(2), 0, 0	0.0198(8)	0.0312(10)	0.0204(7)

Fourier coefficients of the modulation functions

	u _x ^S	u _y ^S	u _z ^S	u _x ^C	u _y ^C	u _z ^C
Rh	1. order					
	0	0	-0.0621(5)	0	0	0
	2. order					
	0	0	0.0255(6)	0	0	0
Sr	-0.0141(2)	0	0	0	0	0
As	-	0	0.0278(3)	0.01391(17)	0	0.0227(2)
	0.01136(14)					

Crenel function width centre

Rh	1	0.5
----	---	-----

Coefficients of the modulation function of the ADP parameters

Atom	term	U ₁₁	U ₂₂	U ₃₃
Rh	s	0	0	0
	c	-0.0000(9)	0.0034(8)	0.00442(15)
Sr	s	0	0	0
	c	0	0	0
As	s	-0.0040(9)	-0.0220(6)	-0.0081(4)
	c	0.0049(12)	0.0269(7)	0.0099(5)
		U ₁₂	U ₁₃	U ₂₃
Rh	s	0.0013(6)	0	0
	c	0	0	0
Sr	s	0	0	0
	c	0	-0.0015(6)	0
As	s	0	-0.0079(7)	0
	c	0	-0.0064(5)	0

Table 5 crystallographic data of α -SrRh₂As₂ in the multiphase refinement

Atom	x	y	Z	U _{iso}
Sr1	0.246(2)	0.757(2)	0.1294(11)	0.020(3)
Rh1	0.215(3)	0.5007(13)	0.3911(15)	0.0104(19)
Rh2	0.308(5)	0.0046(14)	0.348(2)	0.028(2)
As1	0.207(4)	0.4015(15)	0.128(2)	0.038(5)
As2	0.273(3)	0.1244(11)	0.1169(16)	0.021(3)
twinning matrices: β -phase to α -phase				
1. (0 1 0 -0.5 0 -1 -0.5 0 1)				
2. (0 -1 0 -0.5 0 -1 0.5 0 -1)				

Figure 7 shows the modulated structure of β - SrRh_2As_2 (view along the b -axis, three unit cells in c -direction are shown). Both the slight modulations of As and Sr in c -direction and the modulations of the ADP parameters are visible. Fig. 8c illustrates the modulation within the RhAs_4 tetrahedra planes (only the Rh atoms are shown). The modulation leads to a strong elongation of every seventh Rh-Rh distance to 358.0 pm along c , while the adjoining distances have a length of 313.2 pm and 295.8 pm and the shorter ones as well as all distances parallel to b remain close to 287 pm. Fig. 8b shows the t -plot of the Rh-Rh distances. As expected, the biggest change of the Rh-Rh distances takes place near the “jump” of the Rh modulation function. The Rh-As distances (t -plot shown in Fig. 8a) vary from ~ 227 pm to 257 pm, the variation is bigger than in α - SrRh_2As_2 . Both the minimal and maximal distances occur near the jump of the modulation function of the Rh-atom, as the As atoms adjust to their bonding partner. Near this point, also enlarged atomic displacement parameters are observed (Fig. 7).

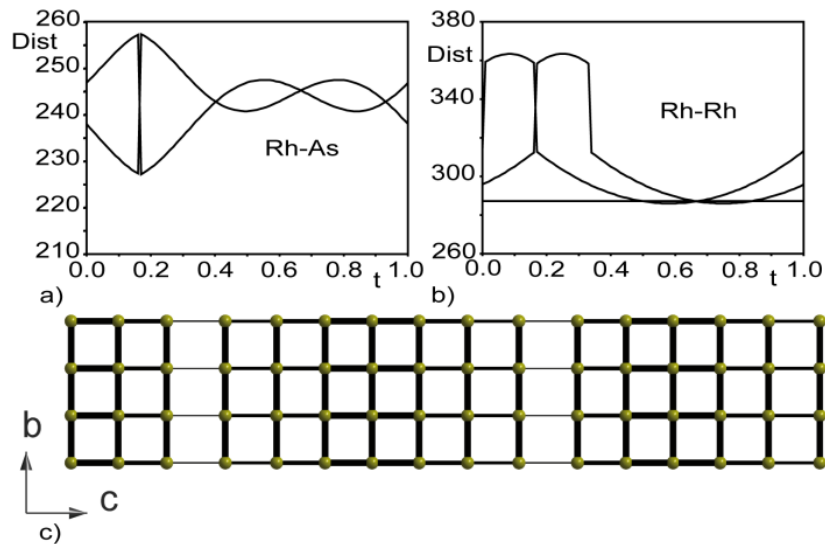


FIG. 8. a) t -plot of the Rh-As distances (pm), b) t -plot of the Rh-Rh distances (pm), c) Rh-Rh network in β - SrRh_2As_2 , elongated distances are shown with thinner lines

This model describes the essential characteristics of the modulated structure of β - SrRh_2As_2 , even though the much weaker satellite reflections with $\mathbf{q} = (0.5, 0, \approx 1/6)$ are still neglected. These will probably allow to describe the modulation in more detail, and maybe help to improve both displacement parameters and Rh-As distances close to the jump of the modulation. However, due to the very weak intensity of these spots, we were not able to measure them with the accuracy required to improve our model.

Previous publications¹⁷ mentioned the β -phase as a high temperature polymorph stable between about 190 and 282 °C. We confirm these results as we could observe the phase transition from α - to β - phase with high temperature powder diffraction. A flux synthesized crystal of β - SrRh_2As_2 showed still the same satellite reflections found at room temperature at 290 °C, but the quality was not sufficient for further x-ray analysis. Upon cooling, the crystal transformed to α - SrRh_2As_2 . The α -phase is the stable polymorph at room temperature, which is nicely supported by the fact that β - SrRh_2As_2 easily transforms to α - SrRh_2As_2 at room temperature under pressure of approximately 1-2 GPa in a hand press (Fig. 9). The fraction of α -phase in the single crystal of β - SrRh_2As_2 used for structure determination increased from 7 % to about 30 % within one year at ambient conditions. Magnetic susceptibility measurements from 300 to 1.8 K on a sample of β - SrRh_2As_2 with some fraction of α - SrRh_2As_2 showed values typical for a Pauli-paramagnetic metal, although some traces of ferromagnetic impurity were observed.

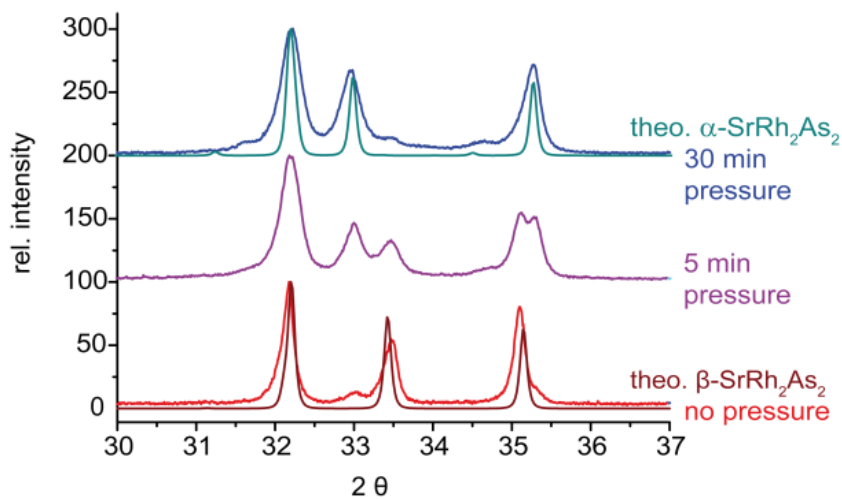


FIG. 9. β - SrRh_2As_2 transforms to α - SrRh_2As_2 under pressure

3. γ - SrRh_2As_2

Several attempts to obtain powder samples or single crystals of γ - SrRh_2As_2 by quenching from high temperatures remained unsuccessful, but the diffraction pattern of a β - SrRh_2As_2 crystal measured at 350 °C showed tetragonal symmetry. As described in the literature¹⁷ γ - SrRh_2As_2 crystallizes in the tetragonal ThCr_2Si_2 -type structure (Table 6). The lattice parameter c is 1156.1(3) pm at 350 °C, thus elongated compared to 1143.1(6) pm as reported for the γ -phase at room temperature.¹⁷ Also the ADP parameters are enlarged due to the higher temperatures.

Table 6. Crystallographic data of γ -SrRh₂As₂ at 350 °C

Empirical formula	SrRh ₂ As ₂
Crystal system, space group	Tetragonal, <i>I4/mmm</i> , No. 139
<i>a</i> , <i>c</i> (pm)	412.68(6), 1156.1(3)
Cell volume (nm ³)	0.19688(6)
Molar mass (g/mol)	443.3
Calculated density (g/cm ³), <i>Z</i>	7.477, 2
Radiation type, λ (Å)	Ag-K α , 0.56087
Temperature (K)	623
2θ range	4.6 - 60.9
Transmission (min, max)	0.0605, 0.6104
Absorption coefficient (mm ⁻¹)	20.32
Total number of reflections	2268
Independent reflections, R_{int}	213, 0.1229
Reflections with $I > 2\sigma(I)$, R_{σ}	168, 0.0604
Refined parameters, Goodness-of-Fit on F^2	8, 1.158
$R1, wR2$ ($I > 2\sigma(I)$)	0.0376, 0.1392
$R1, wR2$ (all data)	0.0516, 0.1623
Largest residual peak, hole $e^{-}/\text{\AA}^3$	4.164, -1.494
Atomic parameters	
Sr	$2a$ (0,0,0) $U_{eq} = 0.0211(4)$
Rh	$4d$ (0,0.5,0.25) $U_{eq} = 0.0286(4)$
As	$4e$ (0,0, z) $z = 0.3637(2)$ $U_{eq} = 0.0255(4)$

B Electronic structure and discussion

The distortions of the ThCr₂Si₂-type structure in SrRh₂As₂ mainly affect the Rh-Rh bonds within the RhAs₄-layer, while the changes of other bond lengths may be regarded as consequences of that. It seems probable that the origin of the polymorphism lies in the Rh-Rh bonding situation, which has been analyzed by the Crystal Orbital Hamilton Population (COHP) method. Fig. 10 shows COHP curves of the Rh-Rh bonds in tetragonal γ -SrRh₂As₂ with ThCr₂Si₂-type structure and monoclinic α -SrRh₂As₂. For γ -SrRh₂As₂ (Fig. 10a), the calculations show strongly Rh-Rh antibonding states around the Fermi energy E_F , caused by $dd\sigma^*$ -type interactions of the in-plane rhodium orbitals within the square network as shown in Fig. 2 (right). As those interactions are quite unfavourable, one would expect the situation to be improved in the low temperature phases. The very similar situation of SrRh₂P₂ has been analyzed earlier in detail.²⁰ If we look at the structural changes within this Rh-Rh network for the low temperature phases, we first find the distortion from tetragonal to orthorhombic in β -SrRh₂As₂. The additional modulation causes strong elongations of several Rh-Rh-bonds (Fig. 8c). Every seventh bond along *c* is stretched to

358.0 pm, with the adjoining bonds elongated slightly to 313.2 and 295.8 pm. All other bonds in this direction and all bonds along b are almost the same as in the γ -phase, with 287.12 pm and 287.4 pm compared to 290 pm in γ -SrRh₂As₂. This elongation of several bonds without much shortening of others is also reflected by the lattice parameters: The identical diagonals in the tetragonal γ -phase are $a^*\sqrt{2} = 581.5$ pm, and split into 574.4 pm (-7 pm) and 611.5 pm ($+30$ pm) in the β -phase. The monoclinic distortion in α -SrRh₂As₂ is even more successful in elongating Rh-Rh distances (Fig. 2): every fourth distance is widened to 378 pm. The effect of the structural changes on the bonding situation in α -SrRh₂As₂ can be studied in the Rh-Rh COHP that is shown in Fig. 10 (right). Most of the antibonding states that were present at E_F in γ -SrRh₂As₂ have been lowered in energy, and are thus less unfavourable. This can be considered as a typical CDW scenario, where compounds compensate highly symmetric but unfavourable bonding situations by splitting bonds in longer and shorter ones yielding lower symmetry structures. More detailed calculations and analysis of the electronic structure including the Fermi surface topology are still necessary to obtain details of a CDW scenario, but are beyond the scope of this article.

In spite of some similarities, this situation is clearly different from that in BaFe₂As₂, where the orthorhombic distortion is much smaller and intimately connected to magnetic interactions. Our results suggest that the much more pronounced effect in SrRh₂As₂ is caused by the larger overlap of the in-plane $4d$ -orbitals responsible for strong Rh-Rh bonding. The higher electron count of SrRh₂As₂ places the Fermi-level just in the middle of the Rh-Rh antibonding $dd\sigma^*$ -bands which can be stabilized by splitting in a structure with lower symmetry. This is different in BaFe₂As₂, where the Fermi-level cuts Fe-Fe antibonding bands of $dd\pi^*$ character that overlap too weak to cause a strong lattice distortion.

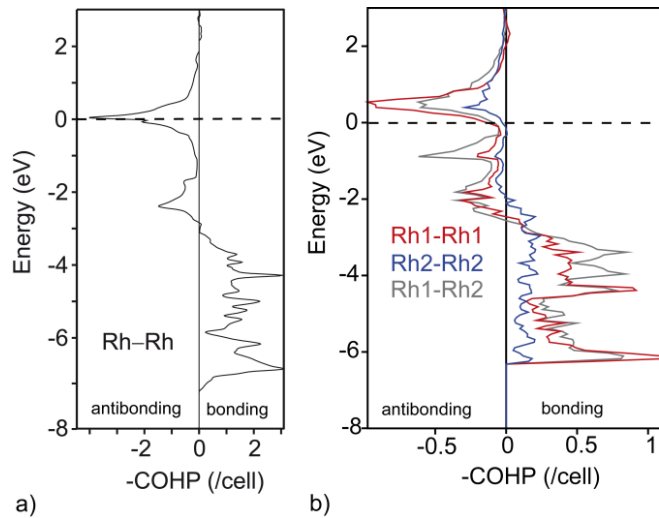


FIG. 10. a) Rh-Rh-COHP of tetragonal γ -SrRh₂As₂ b) Rh-Rh-COHP of monoclinic α -SrRh₂As₂

IV Conclusions

In summary, we have synthesized single crystals and powder samples of SrRh_2As_2 and studied the structures of three polymorphs in detail. We solved the up to now unknown structure of α - SrRh_2As_2 that crystallizes in the monoclinic space group $P2_1/c$ with $a = 421.2(1)$ pm, $b = 1105.6(2)$ pm, $c = 843.0(1)$ pm and $\beta = 95^\circ$ and is twinned. We revealed that the previous structural model for β - SrRh_2As_2 only describes the average structure. A structural modulation with $\mathbf{q} = (0.5, 0, 0.1655)$ was found, where second order satellites are much stronger than first order satellites. Taking into account the strong satellites we present an incommensurate structure in the (3+1) dimensional superspace group $Fmmm(10\gamma)\sigma 00$ with the unit cell parameters $a = 1114.4(3)$ pm, $b = 574.4(2)$ pm and $c = 611.5(2)$ pm and a modulation vector $\mathbf{q} = (1, 0, 0.3311(4))$. The strong modulation of the Rh atom could be described by a crenel function and leads to a variation of the Rh-Rh distances along c from 287 pm to 358 pm. For the γ -phase, high temperature single crystal data confirm the ThCr_2Si_2 -type structure of γ - SrRh_2As_2 as reported in literature. Our DFT calculations with COHP bonding analysis show that distortion and elongation of Rh-Rh bonds lead to lowering in energy of antibonding states in α - SrRh_2As_2 compared to tetragonal γ - SrRh_2As_2 , thus the driving force of the lattice distortions comes from Rh-Rh bonding and has no magnetic origin as suggested for BaFe_2As_2 .

Acknowledgement

This work was financially supported by the DFG within the priority program SPP 1458 “High-Tc superconductivity in iron pnictides” under project JO257/6-1.

Notes and references

*
johrendt@lmu.de

¹G. Grüner, *Density Waves in Solids* (Perseus Publishing, Cambridge, MA, 1994).

²M. Tinkham, *Introduction to Superconductivity* (Dover Publications, Mineola, N.Y., 1996).

³P. Monceau, N. P. Ong, A. M. Portis, A. Meerschaut and J. Rouxel, *Phys. Rev. Lett.* **37**, 602 (1976).

⁴J. A. Wilson, F. J. D. Salvo and S. Mahajan, *Adv. Phys.* **24**, 117 (1975).

⁵E. Canadell and M. H. Whangbo, *Chem. Rev.* **91**, 965 (1991).

⁶M. D. Johannes and I. I. Mazin, *Phys. Rev. B* **77**, 165135 (2008).

⁷D. S. Inosov and *et al.*, *New J. Phys.* **10**, 125027 (2008).

⁸J. G. Bednorz and K. A. Müller, *Z. Phys. B: Condens. Matter* **64**, 189 (1986).

⁹Y. Kamihara, T. Watanabe, M. Hirano and H. Hosono, *J. Am. Chem. Soc.* **130**, 3296 (2008).

- ¹⁰M. Rotter, M. Tegel and D. Johrendt, *Phys. Rev. Lett.* **101**, 107006 (2008).
- ¹¹P. Quebe, L. J. Terbüchte and W. Jeitschko, *J. Alloys Compd.* **302**, 70 (2000).
- ¹²M. Pfisterer and G. Nagorsen, *Z. Naturforsch. B, Chem. Sci.* **35B**, 703 (1980).
- ¹³C. de la Cruz, Q. Huang, J. W. Lynn, J. Y. Li, W. Ratcliff, J. L. Zarestky, H. A. Mook, G. F. Chen, J. L. Luo, N. L. Wang and P. C. Dai, *Nature* **453**, 899 (2008).
- ¹⁴M. Rotter, M. Tegel, I. Schellenberg, W. Hermes, R. Pöttgen and D. Johrendt, *Phys. Rev. B* **78**, 020503(R) (2008).
- ¹⁵I. I. Mazin, D. J. Singh, M. D. Johannes and M. H. Du, *Phys. Rev. Lett.* **101**, 057003 (2008).
- ¹⁶M. Rotter, M. Pangerl, M. Tegel and D. Johrendt, *Angew. Chem. Int. Ed.* **47**, 7949 (2008).
- ¹⁷A. Hellmann, A. Loehken, A. Wurth and A. Mewis, *Z. Naturforsch. B: Chem. Sci.* **62**, 155 (2007).
- ¹⁸M. Tegel, M. Rotter, V. Weiss, F. M. Schappacher, R. Pöttgen and D. Johrendt, *J. Phys.: Condens. Matter* **20**, 452201 (2008).
- ¹⁹I. R. Shein and A. L. Ivanovskii, *Solid State Commun.* **149**, 1860 (2009).
- ²⁰D. Johrendt, C. Felser, O. Jepsen, O. K. Andersen, A. Mewis and J. Rouxel, *J. Solid State Chem.* **130**, 254 (1997).